J. Fluid Mech. (2024), *vol*. 1000, A78, doi:10.1017/jfm.2024.1036

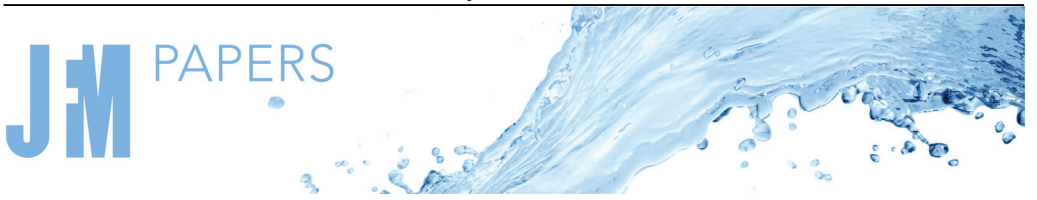

Aerothermodynamics of a sphere in a monatomic gas based on *ab initio* interatomic potentials over a wide range of gas rarefaction: subsonic flows

Felix Sharipov[1],† **and Alexey N. Volkov**[2]

[1]Departamento de Física, Universidade Federal do Paraná, Caixa Postal 19044, Curitiba 81531-980, Brazil

[2]Department of Mechanical Engineering, University of Alabama, 7th Avenue, Tuscaloosa, AL 35487, USA

(Received 31 May 2024; revised 17 September 2024; accepted 19 October 2024)

Aerothermodynamic characteristics of a sphere in a subsonic flow are calculated over a broad range of gas rarefaction by the direct simulation Monte Carlo method based on *ab initio* interatomic potentials and Cercignani–Lampis surface scattering kernel. Calculations of the drag and average energy transfer coefficients are performed for various noble gases in the range of Mach number from 0.1 to 1. The obtained results point out that the influence of the interatomic potential is weak in subsonic flows. A comparison of the present results with a linear theory shows that the numerical solutions at Mach number equal to 0.1 are close to those obtained from the linearized kinetic equation in the transitional and free-molecular regimes. In the near-continuum flow regime, the difference between the present solution and the linear theory is significant. To reveal the effects of the gas–surface accommodation, a few sets of the tangential momentum and normal energy accommodation coefficients are considered in simulations. It is shown that the effect of the accommodation coefficients on the sphere drag is not trivial, and, for non-diffuse scattering, the drag coefficient can be either larger or smaller than that for diffuse scattering. The effect of the sphere temperature is also investigated and the calculated values of the average energy transfer coefficient are used to find the Stanton number, recovery factor and adiabatic surface temperature. The numerical results for the sphere drag and energy transfer are compared with the semi-empirical fitting equations known from the literature.

Key words: rarefied gas flow, aerodynamics, low-Reynolds-number flows

† Email address for correspondence: sharipov@fisica.ufpr.br

1. Introduction

A rarefied gas flow past a sphere is a classical problem of fluid mechanics, which is of fundamental importance for understanding the physics of such phenomena as the transport of aerosols in the atmosphere (Davis 1997), microfluidics (Kim & Yoo 2012), security of nuclear plants (Chen *et al.* 2020), dusty gas flows over bodies (Volkov, Tsirkunov & Oesterlé 2005) and two-phase gas–solid particle jets released from solid rocket motors (Carlson & Hoglund 1964; Galkin, Kogan & Fridlender 1972; Nelson & Fields 1996; Aleksandrov & Fridlender 2008). The motion and heat transfer of spherical microparticles and droplets are common for multiple analytical techniques and technological applications, where laser radiation is used for flow characterization or material processing and fabrication, such as laser-induced incandescence (Liu *et al.* 2006), pulsed laser ablation (Volkov & O'Conner 2011; Volkov & Stokes 2024) and laser powder-bed fusion additive manufacturing (Stokes *et al.* 2022). Laser-induced flows with particles are usually characterized by a large temperature difference between particles and surrounding gas as a result of laser heating of particles and, thus, occur under conditions of the strong coupling between particle drag and heat transfer.

Due to the fundamental nature of this problem, the flow past a sphere can be considered as one of the benchmark problems of rarefied gas dynamics (Sharipov 2012*a*) and can be used to validate various numerical methods and models. This problem has been investigated in depth in the case of supersonic and hypersonic flows. An analysis of corresponding experimental and computational data with relevant references can be found in the paper by Sharipov & Volkov (2022). In particular, near-free-molecular, transitional and near-continuum supersonic flows of monatomic gases over a sphere were studied in kinetic simulations based on the direct simulation Monte Carlo (DSMC) method (Bird 1994), which represents a stochastic particle-based computational approach for solving problems formulated in terms of the Boltzmann kinetic equation.

The case of subsonic flows over a sphere is characterized by overall smaller degrees of rarefaction and non-equilibrium effects since shock waves in this case do not form. At the same time, as was recognized, for example, by Millikan (1910) in his oil droplet experiments, the classical Stokes equation (Stokes 1845, 1851) for the sphere drag obtained for incompressible continuum flows fails to predict the drag force on small spheres at small but finite Mach numbers. As is known, when the Reynolds number is smaller than the Mach number, the gas becomes rarefied. However, in most papers on subsonic flows, the Reynolds number is low but still large enough to treat the flowing gas as a continuous medium. The case of transitional subsonic flows over a sphere presents substantial difficulties for both experimental measurements and direct simulations such as DSMC. Indeed, the relative magnitude of statistical noise in DSMC strongly increases with decreasing Mach number, which requires accumulation of extremely large statistical samples to obtain statistically meaningful results. As a result, the experimental and computational literature data on sphere drag and heat transfer in transitional subsonic flows are very poor. Bailey (1974) reported experimental drag coefficients for the ranges of $Ma < 0.2$ and $Re \geq 0.01$. At larger Reynolds numbers, experimental data for the sphere drag were obtained by Bailey & Hiatt (1971) and Roos & Willmarth (1971). A three-dimensional flow past a rotating sphere at $Ma = 0.2$ was considered in DSMC simulations by Volkov (2009, 2011). Other experimental and computational results for a subsonic sphere drag were summarized by Loth *et al.* (2021), who also developed an accurate semi-empirical equation for the sphere drag coefficient. Another semi-empirical equation for the sphere drag coefficient accounting for the rarefaction and compressibility effects was developed by Henderson (1976). The latter also accounts for the difference

between the sphere and free-stream temperatures. The heat transfer of a sphere at rest in the transitional regime was considered in DSMC simulations by Filippov & Rosner (2000) and Liu *et al.* (2006). The experimental results for the sphere heat transfer in subsonic transitional flows were summarized by Kavanau (1955) and Koshmarov & Svirshevskii (1993), who also developed semi-empirical equations for the sphere Nusselt number and adiabatic temperature. However, the accuracy of such coarse approximations is questionable.

In the case of extremely small Mach numbers, the kinetic equations can be linearized, opening a way for asymptotic solution of rarefied gas dynamics problems (Sharipov 2016). As a result, the flow of a rarefied gas past a sphere in the limit of small Mach number was intensively studied (e.g. Cercignani, Pagani & Bassanini 1968; Beresnev, Chernyak & Fomyagin 1990; Loyalka 1992; Lima Bernardo, Moraes & Rosas 2013; Kalempa & Sharipov 2020, 2022; Taguchi & Tsuji 2022). A similar linearization technique was also used to predict the temperature field around a sphere and local heat transfer when the temperatures of the surface and stream are the same (e.g. Aoki & Sone 1987). Under such conditions, the drag coefficient is proportional to the Mach number, while the average energy transfer coefficient just vanishes. It is quite clear that such solutions cannot be directly extended to the case of finite Mach numbers, and the exact range of applicability of these solutions can be established only by comparing the results of the linear theory with those based on the full kinetic equation.

The aim of the present paper is to calculate aerothermodynamic characteristics of a sphere in the subsonic flow regime over a wide range of gas rarefaction. To this end, systematic simulations of flows using the DSMC method based on *ab initio* potentials (Sharipov & Strapasson 2012) are performed for various noble gases in the range of Mach number from 0.1 to 1. In the simulations, the rarefaction parameter varies in the range from 0 to 10, which spans the free-molecular, transitional and slip-flow regimes. The simulations are targeted at four specific goals, which have not been addressed in the literature. First, we point out the effect of gas species on both drag and heat transfer coefficients. Second, we compare the sphere drag coefficients with the predictions of the linear theory to find the range of applicability of this theory. Third, we study the effects of the incomplete gas–surface accommodation using the scattering model proposed by Cercignani & Lampis (1971) for several sets of tangential momentum accommodation coefficient (TMAC) and normal energy accommodation coefficient (NEAC). Fourth, we consider a broad range of gas–surface temperature ratios to reveal the effects of coupling between sphere drag and heat transfer in subsonic flows.

2. Statement of the problem

In the present work, the problem is formulated in the form that was previously used by Sharipov & Volkov (2022) for supersonic flows over a sphere. A sphere of radius R at rest is streamlined by a dilute gas. Far from the sphere, the equilibrium monatomic gas at pressure p_∞ and temperature T_∞ flows with a constant bulk velocity U_∞ as shown in figure 1. The temperature of the sphere surface T_w can be different from the free-stream temperature T_∞. The primary goal of the simulations is to find the local stress and energy coefficients at the sphere surface, as well as the drag and average energy transfer coefficients for the whole sphere.

The main factors that determine the solution of the problem are the Mach number Ma and rarefaction parameter δ (Sharipov 2016) defined as

$$Ma = \frac{U_\infty}{c_s} \quad \text{and} \quad \delta = \frac{Rp_\infty}{\mu_\infty v_\infty}, \tag{2.1a,b}$$

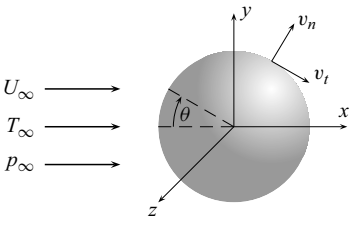

Figure 1. Scheme of the flow.

respectively. Here $c_s = \sqrt{\gamma k_B T_\infty / m}$ is the sound speed, $\gamma = c_p/c_v = 5/3$ is the specific heat ratio, μ_∞ is the gas viscosity at temperature T_∞, $v_\infty = \sqrt{2k_B T_\infty / m}$ is the most probable speed of gas atoms at temperature T_∞, k_B is the Boltzmann constant and m is the mass of a gas atom. The Reynolds number is related to Ma and δ as

$$Re = \frac{2RU_\infty \rho_\infty}{\mu_\infty} = 2\sqrt{\frac{10}{3}}\delta Ma, \tag{2.2}$$

where $\rho_\infty = mp_\infty/(k_B T_\infty)$ is the gas density in the free stream.

The quantities of our interest are the pressure C_p, friction C_f and energy transfer C_h coefficients defined as

$$C_p = \frac{p_n - p_\infty}{\rho_\infty U_\infty^2/2}, \quad C_f = -\frac{\tau}{\rho_\infty U_\infty^2/2}, \quad C_h = -\frac{J_e}{\rho_\infty U_\infty^3/2}, \tag{2.3a–c}$$

where p_n is the stress normal to the sphere surface, τ is the shear stress on the surface and J_e is the energy flux from the surface. The drag C_D and average energy transfer C_Q coefficients are defined as

$$C_D = \frac{F}{\pi R^2 \rho_\infty U_\infty^2/2} = 2\int_0^\pi (C_p \cos\theta + C_f \sin\theta)\sin\theta \, \mathrm{d}\theta, \tag{2.4}$$

$$C_Q = \frac{Q}{2\pi R^2 \rho_\infty U_\infty^3} = \frac{1}{2}\int_0^\pi C_h \sin\theta \, \mathrm{d}\theta, \tag{2.5}$$

where F is the drag force exerted on the sphere and Q is the total energy flux from the gas to the sphere surface.

The coefficients C_D and C_Q are widely used to determine the drag force and energy flux of a sphere in supersonic and hypersonic flows. In subsonic flows at $T_w = T_\infty$, these coefficients diverge as $1/Ma$ when $Ma \to 0$. To avoid this singularity, the computation results in this work are also presented in the form of the reduced coefficients

$$C_i^* = C_i Ma, \quad i = p, f, h, D, Q. \tag{2.6}$$

In addition, at $T_w \neq T_\infty$, the coefficients C_h and C_Q vary inversely proportional to Ma^3 when $Ma \to 0$, so that the energy transfer of the sphere is also characterized by the coefficients

$$C_i^{**} = C_i Ma^3, \quad i = h, Q. \tag{2.7}$$

The solution of the problem is uniquely defined by the Mach number Ma, rarefaction parameter δ, temperature ratio T_w/T_∞ and other similarity parameters that depend on the parameters of the adopted model of binary collisions between gas atoms and model

of gas–surface interaction (Volkov & Sharipov 2017). The binary collisions between atoms of noble gases are described by the solution of the quantum mechanical scattering problem (Joachain 1975) and interatomic interaction potentials established in *ab initio* quantum mechanical calculations as suggested by Aziz, Janzen & Moldover (1995). The simulations are performed for helium (^{4}He), neon and krypton using the interatomic potentials obtained by Cencek *et al.* (2012), Hellmann, Bich & Vogel (2008) and Jäger *et al.* (2016), respectively. For helium, additional test simulations at $Ma = 0.2$ and various δ were also performed using the *ab initio* potential recently found in quantum Monte Carlo simulation by Kayang *et al.* (2023). The simulations based on the potentials by Kayang *et al.* (2023) and Cencek *et al.* (2012) resulted in values of C_D and C_Q that are different by less than 1.5 %. To describe the gas–surface interaction, the model proposed by Cercignani & Lampis (1971) is employed. It includes TMAC and NEAC hereinafter denoted as α_t and α_n, respectively. The main results reported here are obtained assuming the full accommodation on the sphere surface, i.e. diffuse scattering with $\alpha_t = 1$ and $\alpha_n = 1$. Like in the paper by Sharipov & Volkov (2022), the calculations are also performed for helium using two sets of TMAC and NEAC: (i) $\alpha_t = 0.4$ and $\alpha_n = 0.01$; (ii) $\alpha_t = 0.9$ and $\alpha_n = 0.1$. The former corresponds to a treated and polished metal surface, while the latter describes the interaction of helium with a non-treated surface (Sharipov & Moldover 2016). A third set of accommodation coefficients for neon, (iii) $\alpha_t = 0.9$ and $\alpha_n = 0.85$, is used to characterize the effect of the deviations from diffuse scattering, which is observed experimentally for technical surfaces without special treatment (Sharipov & Bertoldo 2006).

The DSMC simulations are performed at $Ma = 0.1$, 0.2, 0.5 and 1 for $\delta = 0.1$, 0.3, 1, 3 and 10 with $T_\infty = 300$ K and sphere temperature T_w equal to 100, 150, 300, 600 and 1000 K. The values of the drag and average energy transfer coefficients at $Ma = 1$ for various δ, $T_\infty = T_w = 300$ K and diffuse scattering obtained previously by Sharipov & Volkov (2022) are used in the present work without changes.

3. Free-molecular and continuum flow limits

The expressions for C_D and C_Q for a sphere in the free-molecular flow regime with the Cercignani–Lampis surface scattering kernel at arbitrary Ma, α_t and α_n were obtained by Sharipov & Volkov (2022) in the form

$$C_D = (1+\alpha_t)\Psi_1(S) + \frac{2}{S^2}\int_{-S}^{S} \xi\, \Phi(\alpha_n, \xi)\, \mathrm{d}\xi, \tag{3.1}$$

$$C_Q = \frac{1}{8}[\alpha_n + \alpha_t(2-\alpha_t)]\left[\Psi_1(S) + \left(1 - \frac{T_w}{T_\infty}\right)\Psi_2(S)\right], \tag{3.2}$$

$$\Phi(\alpha_n, \xi) = \frac{2}{\pi^{3/2} S^2 \alpha_n (T_w/T_\infty)} \int_0^\infty \int_0^\infty \int_0^{2\pi} c^2 c' \times \exp\left(-\frac{c^2 + (1-\alpha_n)c'^2 - 2\sqrt{1-\alpha_n}\, c c' \cos\phi}{\alpha_n (T_w/T_\infty)} - (c'-\xi)^2\right) \mathrm{d}\phi\, \mathrm{d}c'\, \mathrm{d}c, \tag{3.3}$$

$$\Psi_1(S) = \frac{e^{-S^2}}{\sqrt{\pi} S}\left(1 + \frac{1}{2S^2}\right) + \left(1 + \frac{1}{S^2} - \frac{1}{4S^4}\right)\mathrm{erf}(S), \tag{3.4}$$

$$\Psi_2(S) = \frac{2e^{-S^2}}{\sqrt{\pi}S^3} + \left(\frac{2}{S^2} + \frac{1}{S^4}\right)\mathrm{erf}(S), \tag{3.5}$$

where $S = U_\infty/v_\infty$, $\xi = S\cos\theta$ and $\mathrm{erf}(S)$ is the error function. These expressions are consistent with those obtained for a flat plate by Cercignani & Lampis (1972).

The calculations of the drag C_D^* and average heat transfer C_Q^* coefficients with (3.1) and (3.2) as functions of TMAC α_t and NEAC α_n at $Ma = 0.2$ indicate that the variation of α_n has qualitatively different effects on C_D^* and C_Q^* at $T_w/T_\infty = 1$ and $T_w/T_\infty > 1$ (see supplementary material available at https://doi.org/10.1017/jfm.2024.1036). In a nearly isothermal flow at $T_w/T_\infty = 1$, C_D^* decreases and C_Q^* increases with increasing α_n. However, these trends are reversed at $T_w/T_\infty > 1$.

For the purposes of the present work, it is instructive to obtain the series expansions of C_D^*, C_Q^* and C_Q^{**} considering the Mach number Ma as a small parameter. The series expansion of the function $\Phi(\alpha_n, \xi)$ given by (3.3) with respect to ξ takes the form

$$\begin{aligned}\Phi(\alpha_n, \xi) = \Phi_1(\alpha_n) + 2\Phi_2(\alpha_n)\xi + [2\Phi_3(\alpha_n) - \Phi_1(\alpha_n)]\xi^2 \\ + \tfrac{2}{3}[2\Phi_4(\alpha_n) - 3\Phi_2(\alpha_n)]\xi^3 + O(\xi^4),\end{aligned} \tag{3.6}$$

where

$$\begin{aligned}\Phi_m(\alpha_n) = \frac{2}{\pi\alpha_n(T_w/T_\infty)}\int_0^\infty\int_0^\infty\int_0^{2\pi} c^2 c'^m \\ \times \exp\left(-\frac{c^2 + (1-\alpha_n)c'^2 - 2\sqrt{1-\alpha_n}cc'\cos\phi}{\alpha_n(T_w/T_\infty)} - c'^2\right)\mathrm{d}\phi\,\mathrm{d}c'\,\mathrm{d}c.\end{aligned} \tag{3.7}$$

When (3.6) is inserted into (3.1), the terms containing Φ_1 and Φ_3 disappear and only Φ_2 and Φ_4 need to be calculated. In the limit of $\alpha_n \to 0$, the functions Φ_2 and Φ_4 become

$$\Phi_2 = 1, \quad \Phi_4 = 2. \tag{3.8a,b}$$

The extremely small values of $\alpha_n \sim 0.01$ were extracted by Sharipov & Moldover (2016) from the experimental data on the heat flux between helium and machined steel surface reported by Trott *et al.* (2011). Therefore, the limit of $\alpha_n \to 0$ can practically occur. In the opposite limit of $\alpha_n \to 1$, (3.7) reduces to

$$\Phi_2 = \frac{\pi}{4}\left(\frac{T_w}{T_\infty}\right)^{1/2}, \quad \Phi_4 = \frac{3\pi}{8}\left(\frac{T_w}{T_\infty}\right)^{1/2}. \tag{3.9a,b}$$

This limit is typical for heavy gases like krypton.

An expansion of $\Psi_1(S)$ and $\Psi_2(S)$ given by (3.4) and (3.5) with respect to S in combination with (3.6) leads to the following expression for the reduced drag coefficient:

$$C_D^* = 8\sqrt{\frac{2}{15\pi}}\left[1 + \alpha_t + \Phi_2 + \frac{Ma^2}{6}(1 + \alpha_t + 2\Phi_4 - 3\Phi_2)\right] + O(Ma^4). \tag{3.10}$$

Thus, the drag coefficient C_D^* quickly converges to its limit value $8\sqrt{2/(15\pi)}(1 + \alpha_t + \Phi_2)$ at $Ma \to 0$ and arbitrary T_w/T_∞. Even at a relatively large Mach number, the contribution of the term of the order of Ma^2 remains small and, for example, does not exceed 1 % at $Ma \leq 0.3$. The limit value of C_D^* at $Ma \to 0$ agrees with those obtained by Kalempa & Sharipov (2020).

		C_D^*				
α_t	α_n	$Ma \to 0$	$Ma = 0.1$	$Ma = 0.2$	$Ma = 0.5$	$Ma = 1$
0.4	0.01	3.951	3.958	3.978	4.113	4.573
0.4	0.1	3.916	3.922	3.941	4.073	4.519
0.4	0.3	3.841	3.847	3.864	3.986	4.400
0.9	0.1	4.740	4.747	4.771	4.931	5.473
0.9	0.5	4.593	4.600	4.620	4.759	5.233
0.9	0.85	4.475	4.481	4.498	4.615	5.015
1.0	1.0	4.592	4.596	4.613	4.726	5.110

Table 1. Drag coefficient C_D^* versus accommodation coefficients α_t, α_n and Mach number Ma in the free-molecular regime ($\delta \to 0$) at $T_w = T_\infty$.

The series expansions of the energy transfer coefficient C_Q in terms of Ma have different forms in the cases when $T_w = T_\infty$ and $T_w \neq T_\infty$. At $T_w = T_\infty$, the expansion of the coefficient C_Q^* takes the form

$$C_Q^* = \sqrt{\frac{2}{15\pi}}[\alpha_n + \alpha_t(2 - \alpha_t)]\left(1 + \frac{Ma^2}{6}\right) + O(Ma^4). \tag{3.11}$$

This coefficient also quickly converges to its limit value at $Ma \to 0$. At $T_w \neq T_\infty$, the expansion of the coefficient C_Q^{**} results in

$$C_Q^{**} = \sqrt{\frac{2}{15\pi}}[\alpha_n + \alpha_t(2 - \alpha_t)]\left[\left(\frac{18}{5} + Ma^2\right)\frac{T_\infty - T_w}{2T_\infty} + Ma^2\right] + O(Ma^4). \tag{3.12}$$

The differences between (3.11) and (3.12) reflect the fact that, when $T_w \neq T_\infty$ and $Ma \ll 1$, the heat flux is dominated by the temperature difference between the sphere and surrounding gas and only weakly affected by the sphere motion.

The numerical values of the drag coefficient C_D^* in the free-molecular flow regime calculated for $T_w = T_\infty$ and several combinations of α_t and α_n from the expressions obtained by Sharipov & Volkov (2022) are compared with the limit values corresponding to $Ma \to 0$ in table 1. It can be seen that the values of C_D^* at $Ma = 0.2$ are close to those in the limit of $Ma \to 0$ with the difference being smaller than 1 %. These results also demonstrate that the variation of the TMAC and NEAC in the gas–surface interaction model can change C_D^* by 23 %. The largest values of C_D^* correspond to the combination $\alpha_t = 0.9$ and $\alpha_n = 0.1$, while the smallest values of C_D^* are obtained at $\alpha_t = 0.4$ and $\alpha_n = 0.3$.

In the continuum regime ($\delta \to \infty$) and at small Mach number ($Ma \to 0$), the drag coefficient is defined by the Stokes (1851) equation, which is the linearized Navier–Stokes equation. Alternatively, the Stokes equation can be derived from the linearized Boltzmann equation. Taking into account the Oseen (1910, 1913) correction, the drag coefficient is obtained in terms of Ma and δ as

$$C_D^* = \frac{6\sqrt{30}}{5\delta}\left(1 + \frac{\sqrt{30}}{8}\delta Ma\right), \tag{3.13}$$

where (2.2) was used. This expression indicates that the nonlinear correction has the order of δMa and it increases when the rarefaction parameter δ increases.

Thus, the convergence of C_D^* to the linear solution is slow at large values of δ according to (3.13), while the convergence is fast at small δ in agreement with (3.10). The results reported below show the convergence at intermediate values of δ. More detailed analysis of the contribution of the nonlinear terms to the drag coefficient is given by Taguchi & Tsuji (2022), where the series expansion of the Boltzmann equation proposed by Sharipov (2012*b*) was used. To reduce the magnitude of the nonlinear correction below 1 % at $\delta = 10$, the Mach number should be smaller than 10^{-3}. Such small values of Ma are inaccessible by the DSMC method. Therefore, a solution of the full kinetic equation by the discrete velocity method is necessary in order to find the applicability range of the linear theory in the near-continuum regime.

4. Numerical method for the transitional flow regime

Two-dimensional axisymmetric simulations of rarefied gas flows over a sphere in the transitional flow regime are performed using the DSMC method previously applied for supersonic flows over a sphere by Sharipov & Volkov (2022). The sampling of intermolecular collisions in this method is based on the *ab initio* interatomic potentials. The intermolecular collision procedure was previously validated in calculations of viscosity and thermal conductivity by the DSMC method over a wide temperature range (Sharipov 2022).

The high-fidelity DSMC calculations of subsonic flows are challenging and require careful choice of numerical parameters. In simulations, the computational domain represents a cylinder of radius R_d and length $2R_d$ with the sphere placed in its centre. The domain is divided into a regular mesh of cells, where each cell has a shape of a torus of size Δx in the radial and axial directions. The time is discretized and advanced by the time step Δt. The numerical error is determined by the size of the computational domain R_d, cell size Δx, number of modelling particles per cell N_p in the free stream, time step Δt, number of time steps N_{steady} required to establish steady-state flow and number of time steps N_s used to sample parameters of simulated particles for further calculation of macroscopic gas quantities. The optimum values of these parameters were chosen in a series of preliminary simulations. An analysis of the numerical errors and convergence of C_D^* and C_Q^* at variation of numerical scheme parameters are presented in the supplementary material, which shows that the numerical error in the drag coefficient C_D^* does not exceed 0.5 % under all conditions considered here and the numerical error in the average energy transfer coefficient C_Q^* does not exceed 1 % at $Ma \geq 0.2$. It has been found that at $Ma = 0.1$ the fluctuation of C_Q^* in time remains relatively high even after an excessively large number of sampling time steps N_s. In this case, the maximum numerical error of C_Q^* is estimated to be at a level of 1 %–4 %.

The optimum value of each numerical scheme parameter depends on both Mach number Ma and rarefaction parameter δ. The relative size of the computational domain R_d/R and the cell size $\Delta x/R$ for all considered Ma and δ are given in table 2. The time step varies from $\Delta t = 0.002R/v_\infty$ at $\delta = 10$ to $\Delta t = 0.005R/v_\infty$ at $\delta = 0.1$. The number of time steps to establish the steady-state flow is equal to $N_{steady} = N_s/10$. The number of time steps for sampling the flow fields and sphere aerothermodynamic characteristics varies from $N_s = 10^5$ at $Ma = 1$ to 10^7 at $Ma = 0.1$.

	R_d/R				$R/\Delta x$			
δ	$Ma = 0.1$	0.2	0.5	1	$Ma = 0.1$	0.2	0.5	1
0.1	12	12	12	8	20	20	20	20
1	20	20	20	12	20	20	20	20
10	40	30	30	20	60	60	60	60

Table 2. Parameters of the numerical scheme.

	C_D^*				
δ	$Ma \to 0$	$Ma = 0.1$	$Ma = 0.2$	$Ma = 0.5$	$Ma = 1$
0	4.59	4.60	4.61	4.73	5.11
0.1	4.41	4.44	4.45	4.56	4.89
0.3	4.09	4.13	4.16	4.23	4.51
1	3.15	3.16	3.25	3.41	3.70
3	1.73	1.85	1.99	2.31	2.82
10	0.626	0.818	0.956	1.29	2.07

Table 3. Drag coefficient C_D^* of helium versus Mach number Ma and rarefaction parameter δ for diffuse scattering ($\alpha_t = 1$ and $\alpha_n = 1$) at $T_\infty = T_w = 300$ K. The values for $Ma \to 0$ are taken from Kalempa & Sharipov (2020) and Takata *et al.* (1993). The values for $Ma = 1$ are taken from Sharipov & Volkov (2022).

5. Results and discussion

5.1. *Effects of the gas species and interatomic potential*

In the first series of simulations, the coefficients C_D^* and C_Q^* were calculated at $T_w = T_\infty = 300$ K assuming diffuse scattering on the sphere surface for all three noble gases (helium, neon and krypton) considered here. To reveal the effects of the interatomic potentials, additional simulations were also performed with the hard sphere (HS) molecular model. For the HS model, $C_i^* = C_i^*(Ma, \delta, T_w/T_\infty, \alpha_t, \alpha_n)$ $(i = p, f, h, D, Q)$ so that the results of simulations in the reduced units do not depend on the gas species if the model of diffuse scattering is used.

The numerical values of the drag coefficient C_D^* obtained by the DSMC method for helium are given in table 3. The second column in that table contains the limit values of C_D^* at $Ma \to 0$ obtained by Kalempa & Sharipov (2020) at $\delta = 0.1$, 1 and 10. These limit values were obtained by the discrete velocity method applied to the linearized kinetic model proposed by Shakhov (1968). The limit values of C_D^* at $\delta = 0.3$ and 3 are not available in the literature, so that the values of C_D obtained by Takata, Sone & Aoki (1993) applying the discrete velocity method to the linearized Boltzmann equation were interpolated to complete the second column of table 3. The analysis of the numerical results of C_D^* for other gases and for the HS model showed that the effect of gas species on the drag coefficient C_D^* does not exceed a numerical error of 0.5 % so that these data are omitted here.

The results presented in table 3 show that the linear theory is applicable in a relatively large range of the Mach number when the rarefaction parameter is small. More specifically, when $\delta \leq 1$, the values of C_D^* obtained by the DSMC method at $Ma = 0.1$ coincide with those obtained with the linear theory. However, the discrepancy between these two

		C_Q^*			
Ma	δ	HS	^{4}He	Ne	Kr
0.2	0	0.415	0.415	0.415	0.415
	0.1	0.392	0.383	0.398	0.395
	0.3	0.356	0.365	0.365	0.366
	1	0.252	0.258	0.261	0.263
	3	0.139	0.140	0.141	0.140
	10	0.0713	0.0707	0.0747	0.0758
0.5	0	0.429	0.429	0.429	0.429
	0.1	0.410	0.411	0.410	0.413
	0.3	0.368	0.370	0.371	0.373
	1	0.270	0.270	0.271	0.275
	3	0.155	0.157	0.157	0.161
	10	0.0842	0.0849	0.0838	0.0844
1	0	0.477	0.477	0.477	0.477
	0.1	0.450	0.451	0.452	0.453
	0.3	0.399	0.403	0.403	0.409
	1	0.291	0.297	0.297	0.304
	3	0.176	0.179	0.179	0.184
	10	0.0934	0.0942	0.0942	0.0955

Table 4. Average energy transfer coefficient C_Q^* versus Mach number Ma and rarefaction parameter δ for diffuse scattering ($\alpha_t = 1$ and $\alpha_n = 1$) at $T_\infty = T_w = 300\,\mathrm{K}$.

approaches becomes 7 % at $\delta = 3$ and reaches 27 % at $\delta = 10$. This trend is consistent with the analytical expressions (3.10) and (3.13).

As mentioned above, the total energy flux Q to the sphere used in the definition of C_Q^*, equation (2.5), vanishes in the limit of $Ma \to 0$. More exactly, it exhibits asymptotic behaviour $Q \propto Ma^2$ when $Ma \to 0$. This explains why an accurate calculation of C_Q^* at small Ma is a difficult problem due to the statistical noise inherent for the DSMC method. As a result, it was not possible to reach a reasonable accuracy in calculation of C_Q^* at $Ma = 0.1$; therefore, the corresponding results are not shown here. The coefficient C_Q^* for $Ma = 0.2$ and 0.5 for diffuse scattering and $T_w = T_\infty = 300\,\mathrm{K}$ is given in table 4 for the three noble gases and the HS model. Like C_D^*, the coefficient C_Q^* is also weakly affected by the gas species, but the contribution of this factor is about 4 %, which exceeds the estimated numerical error of 1 %. According to (3.11), the contribution of the quadratic term ($\sim Ma^2$) to C_Q^* in the free-molecular flow regime is about 4 % at $Ma = 0.5$. A comparison of the values of C_Q^* for $Ma = 0.2$ and 0.5 in table 4 shows that the contribution of the quadratic term to C_Q^* remains within 4 % also for finite δ in the range $0 \le \delta \le 1$. This contribution increases for larger values of δ and reaches 16 % at $\delta = 10$. The contribution of the quadratic term to C_Q^* at $Ma = 0.2$ is expected to be equal to 0.7 % at $\delta \le 1$ and 2.5 % when $1 < \delta \le 10$. Based on these reasonings, the values of C_Q^* obtained for $Ma = 0.2$ can be also used as a good approximation for C_Q^* at smaller Ma. The values of the average energy transfer coefficient for all gases considered in table 4 at $Ma = 1$ were obtained by Sharipov & Volkov (2022).

5.2. *Effect of the surface accommodation coefficients*

The values of the coefficients C_D^* and C_Q^* obtained for helium with sets (i) and (ii) of the accommodation coefficients, for neon with set (iii) and for krypton with diffuse scattering are compared in figure 2. The horizontal lines in these plots show the values of C_D^* for free-molecular flows ($\delta = 0$) given in table 1 and C_Q^* calculated from (3.11). Note that the difference in the values of C_D^* and C_Q^* for different gases occurs only due to the different sets of accommodation coefficients. If the corresponding values of C_D^* and C_Q^* were to be plotted for the same parameters of the gas–surface interaction model, e.g. for the model of diffuse scattering, the curves for different gases would visually coincide in the scale of figure 2. Set (ii) leads to the largest values of the drag coefficient C_D^*, while set (i) corresponds to the smallest C_D^*. Set (iii) represents a small deviation from the results obtained for diffuse scattering. In the near-continuum flow regime when $\delta = 10$, sets (ii) and (iii) result in practically the same values of C_D^*. The energy transfer coefficient C_Q^* is largest for diffuse scattering. This coefficient always decreases with decreasing either TMAC α_t or NEAC α_n. The expression given by (3.11) shows that the coefficient C_Q^* in the free-molecular flow regime is proportional to $\alpha_n + \alpha_t(2 - \alpha_t)$. This explains the largest value of C_Q^* for diffuse scattering. The effect of the parameters of the gas–surface interaction model becomes weaker with approaching the continuum flow regime, when the rarefaction parameter δ increases. The values of the drag and average energy transfer coefficients at $Ma = 1$ were obtained by Sharipov & Volkov (2022). These results reveal the same trends in the variation of C_D^* and C_Q^* with α_t, α_n and δ that are seen in figure 2(*b*,*d*) for $Ma = 0.5$.

The distributions of the local pressure C_p^*, friction C_f^* and energy transfer C_h^* coefficients for helium along the sphere surface obtained at $Ma = 0.2$ and 0.5 when $T_w = T_\infty = 300\,\mathrm{K}$ with the model of diffuse scattering and with set (i) of the accommodation coefficients are compared in figure 3. To exclude statistical noise, which can be relatively large in the vicinity of the axis of symmetry, the distributions of parameters along the sphere surface in figure 3 and other figures were fitted by high-order polynomials using the least-squares method. The pressure coefficient C_p^* is strongly sensitive to the accommodation coefficients at $\delta = 0.1$ and 1, but is weakly sensitive at $\delta = 10$. The friction C_f^* and energy transfer C_h^* coefficients are strongly sensitive to the values of the accommodation coefficients at all values of δ considered in figure 3; both C_f^* and C_h^* decrease when the accommodation coefficients α_t and α_n decrease. Moreover, with a decrease in the values of accommodation coefficients, the distributions of C_h^* qualitatively change. For diffuse scattering, the maximum of C_h^* occurs in the forward stagnation point. At $\alpha_t = 0.4$ and $\alpha_n = 0.01$, the maximum of C_h^* is realized at $\theta = 90^\circ$, while the values of C_h^* are practically equal to zero in both stagnation points at $\theta = 0$ and $\theta = 180^\circ$. In the case of non-diffuse scattering, the magnitude of C_h^* is significantly smaller than that for diffuse scattering.

It can be seen that the curves of C_p^* and C_f^* at $Ma = 0.2$ are close to those at $Ma = 0.5$ because both $p_n - p_\infty$ and τ, which define C_p and C_f according to (2.3*a–c*), are proportional to U_∞ at $Ma \to 0$. Therefore, both C_p^* and C_f^* defined by (2.6) asymptotically vary as $O(1)$ with respect to Ma in the limit of $Ma \to 0$. However, the local energy flux J_e, which defines C_h in (2.3*a–c*), is proportional to U_∞ at $Ma \to 0$ like $p_n - p_\infty$ and τ. As a result, the coefficient C_h^* defined by (2.6) asymptotically varies as $O(Ma^{-1})$ at $Ma \to 0$ and, therefore, the quantity C_h^* at $Ma = 0.2$ is substantially larger than that at $Ma = 0.5$ as shown in figure 3.

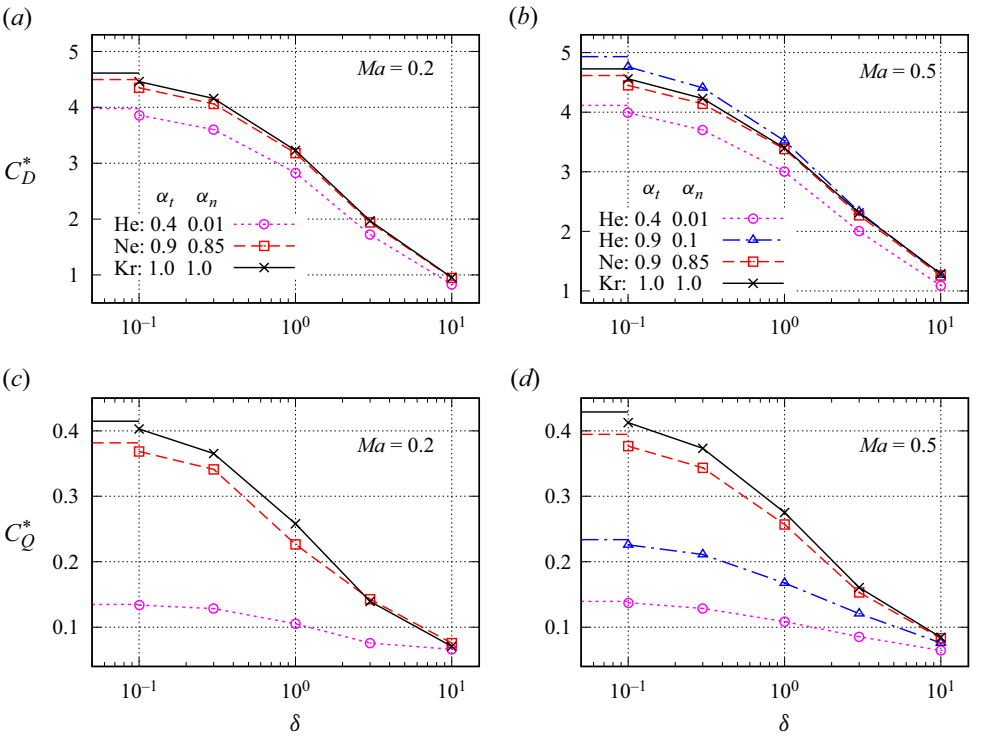

Figure 2. Drag C_D^* and average energy transfer C_Q^* coefficients versus rarefaction parameter δ at $T_\infty = T_w = 300$ K for different sets of α_t and α_n: (*a*,*c*) $Ma = 0.2$; (*b*,*d*) $Ma = 0.5$. The short horizontal lines correspond to the free-molecular flow regime.

In the case of diffuse scattering, the sphere is heated at its front part and cooled at its back part. Moreover, the function $C_h^*(\theta)$ becomes antisymmetric with respect to $\theta = 90^\circ$ at $Ma \to 0$. Such a behaviour of the local energy flux on the sphere surface in the limit of $Ma \to 0$ was pointed out by Beresnev *et al.* (1990) and by Kalempa & Sharipov (2020, 2022). This phenomenon leads to the thermal polarization of a sphere when its thermal conductivity is small. Since the function $C_h^*(\theta)$ becomes antisymmetric at $Ma \to 0$, the average energy flux coefficient C_Q^* is expected to asymptotically behave as $O(1)$ with respect to Ma, in agreement with the numerical results shown in figure 2.

5.3. *Effect of the sphere temperature*

To study the effect of the surface temperature T_w on the aerothermodynamics of a sphere, the DSMC simulations were performed at sphere temperature varying from $T_w = 100$ to 1000 K with the constant free-stream temperature equal to $T_\infty = 300$ K for helium interacting diffusely with the sphere surface. The values of the drag C_D^* and average energy transfer C_Q^{**} coefficients calculated for $Ma = 0.1$, 0.2 and 0.5 and various δ are shown in figure 4. The drag coefficient C_D^* increases with increasing temperature T_w for all Mach numbers and all rarefaction parameters δ. For all T_w considered, the values of C_D^* exhibit a weak dependence on Ma. As expected, the coefficient C_Q^{**} practically linearly decreases with increasing temperature T_w. The negative values of C_Q^{**} mean that the energy is transferred from the sphere to the surrounding gas. The overall effect of Ma on C_Q^{**} is

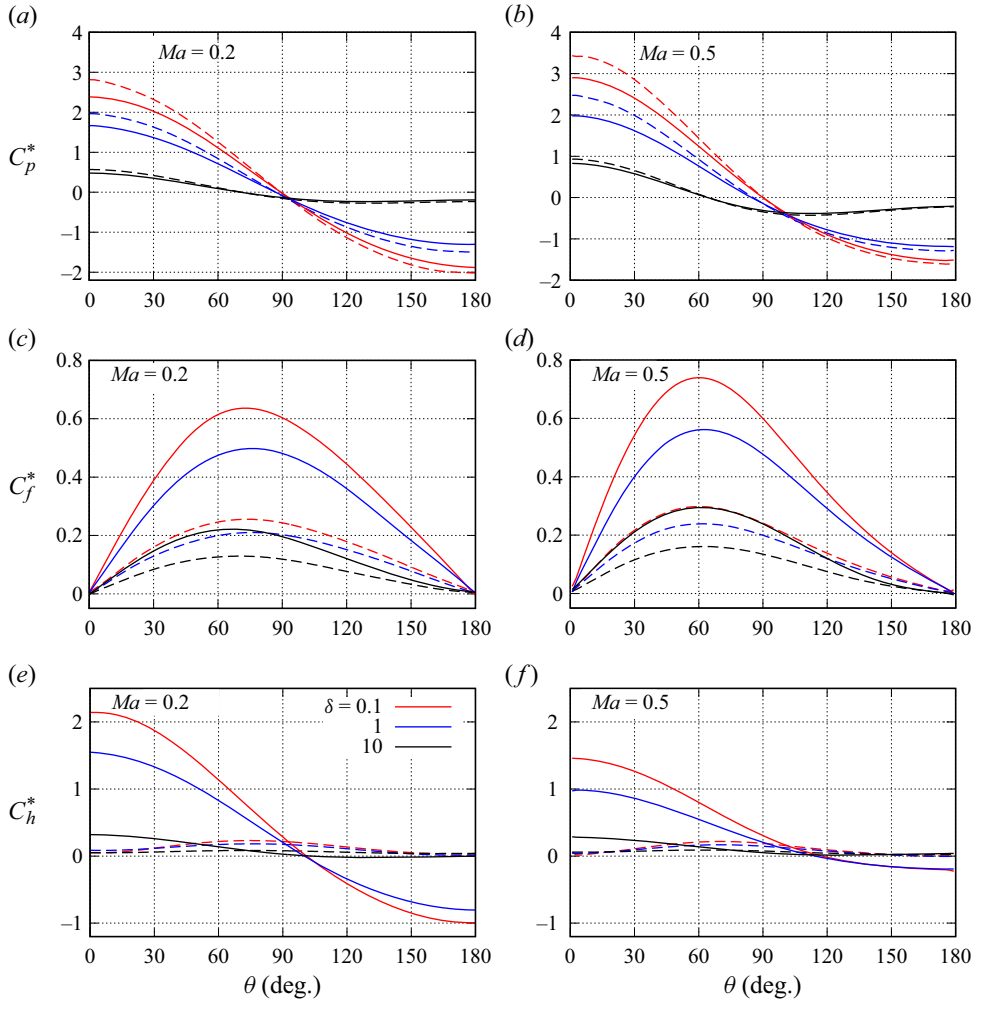

Figure 3. Pressure C_p^*, friction C_f^* and energy transfer C_h^* coefficients versus angle θ at $T_\infty = T_w = 300$ K for helium at various δ: (*a*,*c*,*e*) $Ma = 0.2$; (*b*,*d*,*f*) $Ma = 0.5$. Solid lines, diffuse scattering; dashed lines, $\alpha_t = 0.4$ and $\alpha_n = 0.01$.

also weak. The adiabatic temperature of the sphere which corresponds to $C_Q^{**} = 0$ shifts towards larger values with increasing Ma.

The sphere temperature strongly affects the distributions of C_p^* and C_h^{**} as shown in figures 5 and 6 for $Ma = 0.2$ and $Ma = 0.5$, respectively. An increase of T_w induces an increase of C_p^* at the whole sphere surface, so that the values of C_p^* approach zero and can be even positive at $Ma = 0.2$ in the downstream stagnation point, $\theta = 180^\circ$. At $\delta = 0.1$, the variation of C_p^* with T_w is relatively large for the whole sphere surface. At $\delta = 10$, the effect of T_w on the distribution of C_p^* at the downstream-faced hemisphere becomes relatively weak. The overall effect of T_w on the distribution of C_p^* reduces with increasing Ma. As expected, the effect of T_w on C_h^{**} is strong under all conditions considered. The distributions of the friction coefficient C_f^* are weakly affected by T_w and, therefore, not shown in figures 5 and 6.

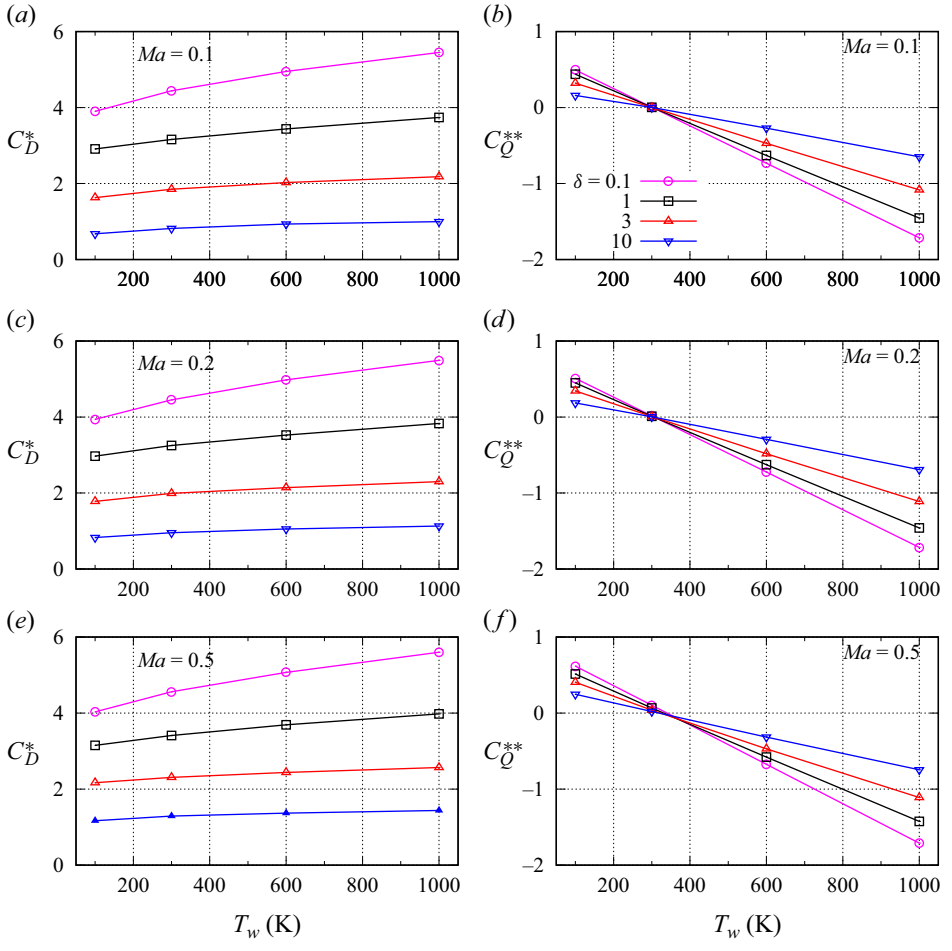

Figure 4. Drag C_D^* and average energy transfer C_Q^{**} coefficients of helium for diffuse scattering versus surface temperature T_w for various Ma and δ.

In figure 7(*a*), the values of the drag coefficient obtained here by the DSMC method with diffuse scattering at $T_w = T_\infty$ are compared with the semi-empirical equations for C_D proposed by Henderson (1976) and Loth *et al.* (2021), which account for the effects of compressibility and rarefaction. The equation by Loth *et al.* (2021) overall agrees well with the numerical values of C_D in the whole range of δ and Ma considered in simulations, while the equation by Henderson (1976) tends to overestimate C_D in the transitional and free-molecular flow regimes. The values of C_D obtained in the present work at $T_w \neq T_\infty$ are compared with C_D calculated from the equation by Henderson (1976) in figure 7(*b*). Note that the equation by Loth *et al.* (2021) is obtained only for the case $T_w/T_\infty = 1$. In contrast to the semi-empirical equation, the DSMC method predicts a non-negligible effect of T_w/T_∞ on C_D in the transitional and near-continuum regimes when $Re \sim 1$. At smaller Re, the difference in C_D between the semi-empirical equation and DSMC data points fast increases with increasing T_w/T_∞. These results suggest that the equation by Henderson (1976) can be used only at $T_w/T_\infty \leq 1$.

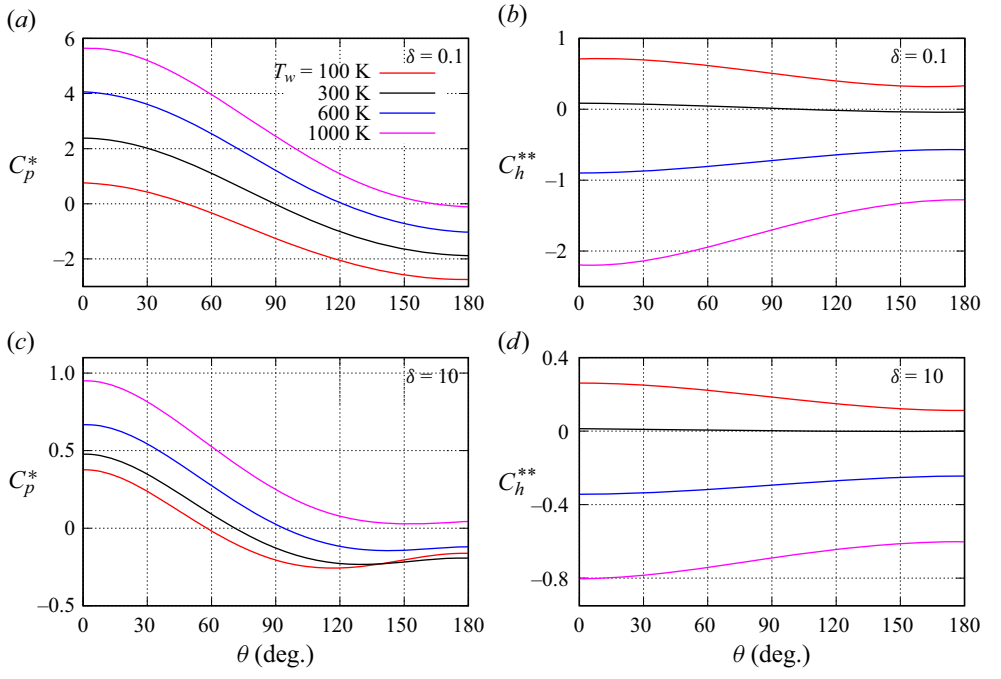

Figure 5. Pressure C_p^* and energy transfer C_h^{**} coefficients of helium for diffuse scattering versus angle θ for $Ma = 0.2$ and various sphere temperatures T_w: (*a*,*b*) $\delta = 0.1$; (*c*,*d*) $\delta = 10$.

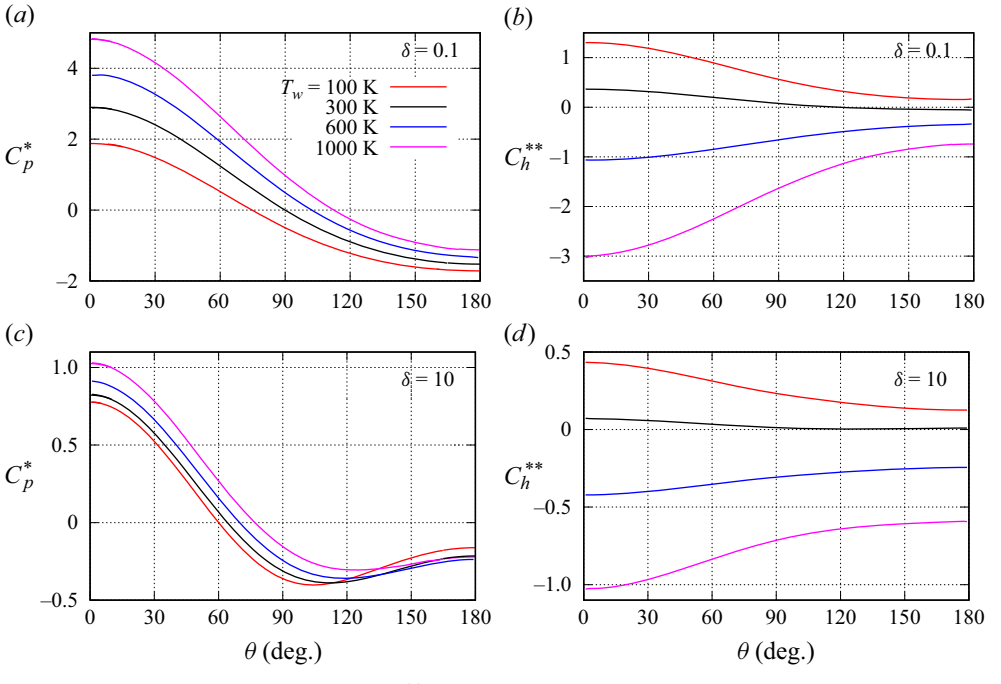

Figure 6. Pressure C_p^* and energy transfer C_h^{**} coefficients of helium for diffuse scattering versus angle θ for $Ma = 0.5$ and various sphere temperatures T_w: (*a*,*b*) $\delta = 0.1$; (*c*,*d*) $\delta = 10$.

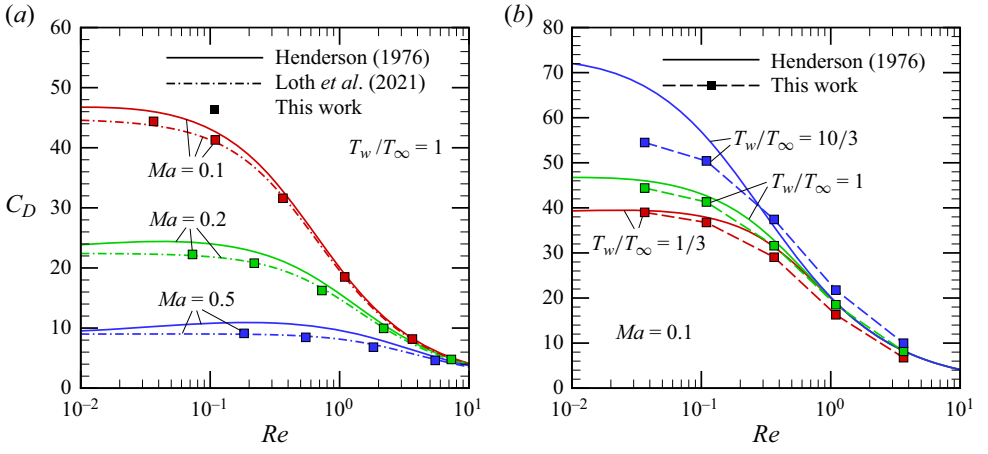

Figure 7. Drag coefficient C_D versus Reynolds number Re predicted by the semi-empirical equation of Henderson (1976) (solid curves), the semi-empirical equation of Loth *et al.* (2021) (dashed-dotted curves) and obtained in the present work (symbols and dashed curves): (*a*) $T_w = T_\infty$ and various Ma; (*b*) $Ma = 0.1$ and various T_w. The DSMC results correspond to helium with diffuse scattering at $T_\infty = 300$ K.

5.4. *Flow fields*

The fields of the gas density n/n_∞, temperature T/T_∞ and speed u/U_∞ ($u = |\boldsymbol{u}|$, where $\boldsymbol{u}$ is the bulk velocity) with streamlines in the flow of helium over the sphere obtained with $T_w = T_\infty = 300$ K and diffuse scattering at $Ma = 0.2$ and $Ma = 0.5$ are shown in figures 8 and 9, respectively. These fields are the typical subsonic flow fields over a thermally neutral sphere in the near-free-molecular ($\delta = 0.1$) and near-continuum ($\delta = 10$) flow regimes. All flow fields shown in figures 8 and 9 are characterized by the smooth variation of all quantities and by the propagation of the perturbations induced by the body to a long distance in the upstream direction. At $Ma = 0.2$ and $T_w/T_\infty = 1$, the density and temperature fields indicate that the flows in this case are nearly incompressible and practically isothermal. The marginal variation of T makes the accurate calculations of the temperature field and C_Q^* at $Ma \leq 0.2$ computationally challenging. At $\delta = 0.1$, the density and velocity fields visually are nearly symmetric with respect to the plane $x = 0$. This qualitatively agrees with the linearized solution for the flow over a sphere at $Ma \ll 1$ obtained by Kalempa & Sharipov (2020). With increasing δ, the flow field attains significant asymmetry with an extended wake behind the sphere.

It is interesting that, in the subsonic flows at $Ma = 0.2$ and 0.5, the maximum of gas temperature in the nearly continuum flow at $\delta = 10$ is located inside the flow fields at the same point as where it is located in the supersonic flow at $Ma = 2$, as reported previously by Sharipov & Volkov (2022). At the axis of symmetry, the temperature maximum is realized at a distance of $0.5R$ upstream from the stagnation point. Another local maximum of temperature is located at the axis of symmetry at a distance of $x \approx 2.4R$ downstream the sphere. The temperature minimum is also located inside the flow field near the cross-section $x = 0$ at a distance of $\approx 1.5R$ from the sphere centre. In comparison with the case of $Ma = 0.2$, the flow at $Ma = 0.5$ is characterized by a significantly higher temperature in front of the sphere and deeper drop of the gas density behind it.

The variation of the sphere surface temperature activates compressibility effects and can strongly affect the flow fields even in subsonic flows at small Ma. To illustrate this, the flow fields obtained at $T_w = 1000$ K and $Ma = 0.2$ for $\delta = 0.1$ and 10 are shown in

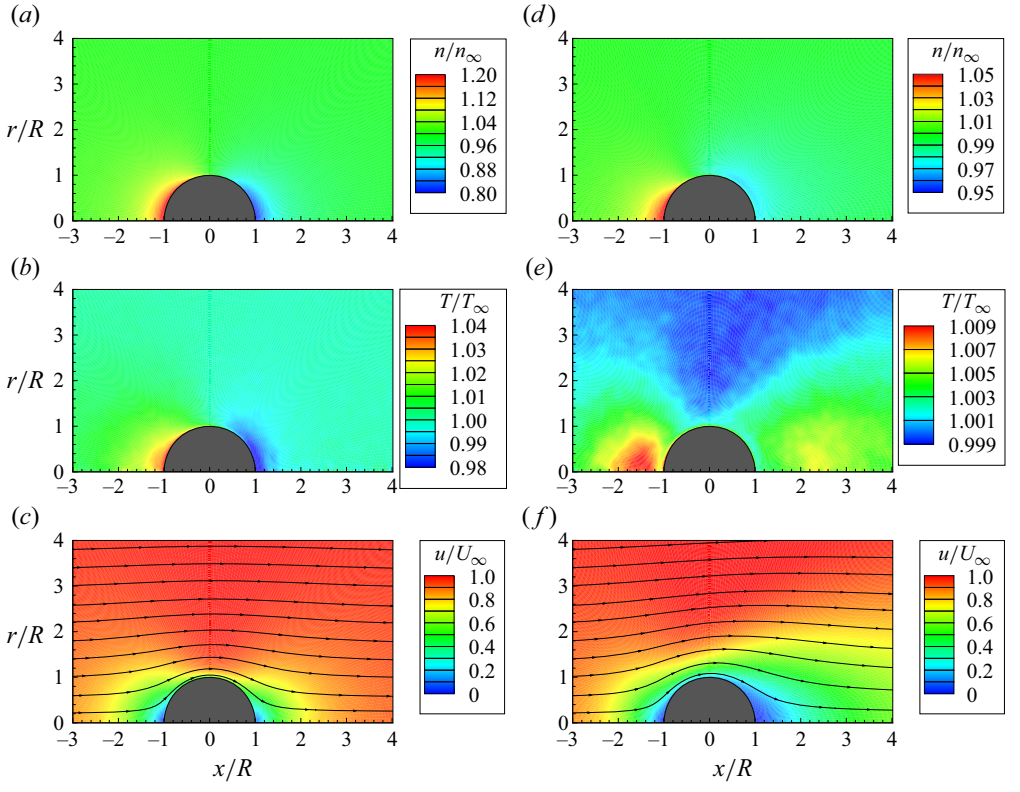

Figure 8. Fields of density n/n_∞ (*a*,*d*), temperature T/T_∞ (*b*,*e*) and speed u/U_∞ with streamlines (*c*,*f*) for helium at $Ma = 0.2$, diffuse scattering and $T_\infty = T_w = 300$ K: (*a–c*) $\delta = 0.1$; (*d–f*) $\delta = 10$.

figure 10. These fields can be compared with the fields obtained under identical conditions but at $T_w = 300$ K (figure 8). An increase in the surface temperature above T_∞ results in an increase of the gas temperature around the sphere and corresponding decrease in the gas number density, which is dictated by preserving gas pressure. The temperature-induced effects remain relatively small in magnitude in near-free-molecular flow at $\delta = 0.1$. In particular, the region of strong variation of the gas temperature is limited by the distances of $\approx 1.4R$ from the sphere centre and the velocity field retains approximate symmetry with respect to the plane $x = 0$. At $\delta = 10$, the region with strong temperature variations extends far beyond in the downstream direction. The fields of n and T tend to be spherically symmetric with decreasing Ma, and, thus, qualitatively different from the corresponding fields at $T_w = T_\infty$. With increasing T_w, the disturbed field of gas velocity u becomes more extended in front of the sphere in the upstream direction so that the disturbances in the gas flow from the heated sphere propagate further than in the case of $T_w = T_\infty$. A decrease of T_w with respect to T_∞ induces opposing changes in the flow field: a decrease of the gas temperature around the sphere, increase of the number density and less extended disturbed velocity field in front of the sphere (see the supplementary material).

5.5. *Stanton number, adiabatic sphere temperature and recovery factor*

In compressible gas flows, the energy flux to the body surface is often represented in the dimensionless form by the Stanton number. For a sphere, the total energy flux Q to its

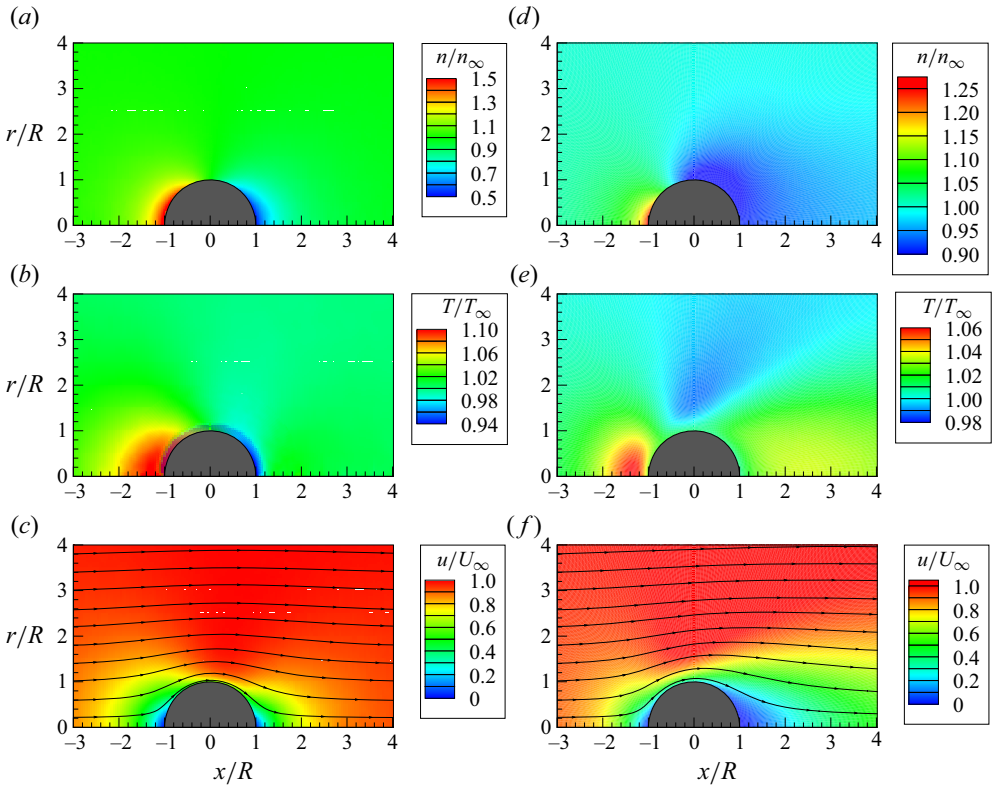

Figure 9. Fields of density n/n_∞ (*a*,*d*), temperature T/T_∞ (*b*,*e*) and speed u/U_∞ with streamlines (*c*,*f*) for helium at $Ma = 0.5$, diffuse scattering and $T_\infty = T_w = 300$ K: (*a*–*c*) $\delta = 0.1$; (*d*–*f*) $\delta = 10$.

surface can be represented as

$$Q = 4\pi R^2 \rho_\infty U_\infty c_p T_\infty St \left(\frac{T_{ad}}{T_\infty} - \frac{T_w}{T_\infty} \right), \tag{5.1}$$

where St is the Stanton number and T_{ad} is the adiabatic sphere temperature, i.e. the homogeneous surface temperature, when the total energy flux from the surface is equal to zero. The relationship between C_Q, St and T_{ad}/T_∞ is given by (2.5) and (5.1).

If the gas species, interatomic potential and accommodation coefficients of the Cercignani–Lampis gas–surface interaction model are fixed, then T_{ad}/T_∞ is a function of Ma and δ, while St depends on Ma, δ and T_w/T_∞. In the free-molecular regime for diffuse scattering, St is given by the equation

$$St = \frac{1}{5\sqrt{\pi}S^2} \left[\sqrt{\pi} \left(S^2 + \frac{1}{2} \right) \mathrm{erf}(S) + S \exp(-S^2) \right], \tag{5.2}$$

where $S = U_\infty/v_\infty = \sqrt{10/3}Ma$. The ratio T_{ad}/T_∞ can be represented in the form

$$\frac{T_{ad}}{T_\infty} = 1 + \frac{2}{5} S^2 \zeta, \tag{5.3}$$

where ζ is the recovery factor defined as

$$\zeta = \frac{T_{ad} - T_\infty}{T_0 - T_\infty}, \tag{5.4}$$

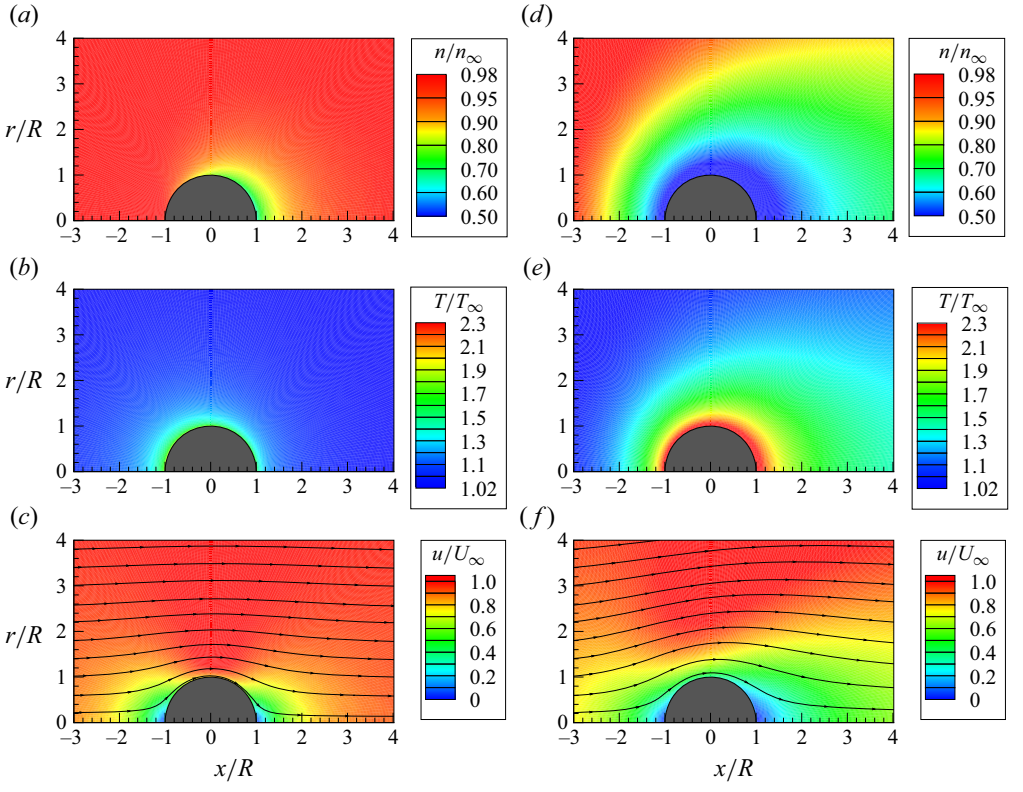

Figure 10. Fields of density n/n_∞ (*a*,*d*), temperature T/T_∞ (*b*,*e*) and u/U_∞ with streamlines (*c*,*f*) for helium at $Ma = 0.2$, diffuse scattering, $T_\infty = 300$ K and $T_w = 1000$ K: (*a*–*c*) $\delta = 0.1$; (*d*–*f*) $\delta = 10$.

and $T_0 = T_\infty[1 + (2/5)S^2]$ is the isentropic stagnation temperature. The dimensionless recovery factor is a measure of the difference of the adiabatic body temperature from the isentropic stagnation temperature. This difference depends on the efficiency of collisional equilibration of gas molecules moving to and from the body surface. The value of ζ can be considered as another integral measure of the degree of gas rarefaction in the rarefied gas aerodynamics as it varies for bodies of various shapes from values larger than 1 in free-molecular flows to values smaller than 1 in continuum flows. In the free-molecular regime, the recovery factor for a sphere takes the form

$$\zeta = \frac{5}{4S^2}\left[\left(S^2 + \frac{1}{2}\right) - \frac{\sqrt{\pi}\,\mathrm{erf}(S)}{\sqrt{\pi}\,(2S^2+1)\,\mathrm{erf}(S) + 2S\exp(-S^2)}\right]. \tag{5.5}$$

At finite δ, the dependence of C_Q^* on multiple flow parameters is relatively complex. The analysis of T_{ad}/T_∞ and St allows one to reveal universal trends that control the variation of C_Q as a function of multiple flow parameters. For this purpose, the values of C_Q^* obtained with the DSMC method for helium and shown in figure 4 are recalculated into the values of St and T_{ad}/T_∞.

The values of T_{ad} are determined first as the surface temperatures when $Q = 0$. Since the variation of C_Q^{**} with T_w is practically linear (figure 4), T_{ad} can be obtained by the linear

interpolation of C_Q^{**} between two points corresponding to temperatures $T_{w(1)}$ and $T_{w(2)}$:

$$T_{ad} = \frac{T_{w(1)} C_{Q(2)}^{**} - T_{w(1)} C_{Q(1)}^{**}}{C_{Q(2)}^{**} - C_{Q(1)}^{**}}, \tag{5.6}$$

where $C_{Q(k)}^{**}$ is the average energy transfer coefficient obtained at $T_w = T_{w(k)}$ and $C_{Q(1)}^{**} \times C_{Q(2)}^{**} < 0$. Since $T_{ad}/T_\infty > 1$ and, for $Ma \leq 1$, $T_{ad}/T_\infty < 2$, (5.6) is used at $T_{w(1)} = 300\,\mathrm{K}$ and $T_{w(2)} = 600\,\mathrm{K}$. The obtained raw values of $\Delta T_{ad} = T_{ad}/T_\infty - 1$ are shown in figure 11(*a*). These results indicate a monotonic decrease of ΔT_{ad} with δ and increase with Ma. In the transitional regime, the magnitude of ΔT_{ad} varies roughly inversely proportional to Ma^2 in agreement with (5.3) for the free-molecular regime. The numerical values of T_{ad}/T_∞ are compared with the predictions based on the semi-empirical equation proposed by Koshmarov & Svirshevskii (1993) to describe the adiabatic temperature of a sphere under a broad range of conditions, including the free-molecular, transitional and continuum flow regimes, in the supplementary material. This comparison showed that the semi-empirical equation systematically overestimates T_{ad}/T_∞ compared with the DSMC results.

The recovery factor for a monatomic gas $\zeta = 3(T_{ad}/T_\infty - 1)/Ma^2$ obtained from (5.4) demonstrates a universal behaviour and only weakly depends on Ma as shown in figure 11(*b*). Under conditions of nearly free-molecular regime at $\delta = 0.1$, ζ decreases when Ma increases from 0.2 to 1 in agreement with (5.5) for the free-molecular regime which predicts the values of $\zeta = 1.665$, 1.659, 1.625 and 1.535 for $Ma = 0.1$, 0.2, 0.5 and 1, respectively. On the contrary, in the near-continuum regime at $\delta = 10$, ζ increases when Ma increases from 0.2 to 1. A density parameter of $\delta \approx 0.5$ corresponds to the nexus point where ζ does not change with Ma. The values of ζ at $Ma = 0.1$ are out of these trends presumably due to insufficient accuracy of DSMC simulations in this case.

Once the numerical values of T_{ad}/T_∞ are determined, the values of St can be calculated as

$$St = \frac{\gamma - 1}{2} \frac{C_Q^{**}}{Ma \left(\dfrac{T_{ad}}{T_\infty} - \dfrac{T_w}{T_\infty} \right)}. \tag{5.7}$$

A table with the calculated values of T_{ad}/T_∞ and St is provided in the supplementary material. Since C_Q^{**} weakly depends on Ma, it is expected that $St \cdot Ma$ is a weak function of Ma as well. The dependencies of $St \cdot Ma$ on δ at various Ma and T_w/T_∞ are shown in figure 11(*c–e*). In the limit of the free-molecular regime, $St \cdot Ma$ becomes independent of T_w/T_∞ according to (5.2). In the transitional regime at $\delta < 3$, the calculated values of $St \cdot Ma$ demonstrate a weak dependence on Ma and T_w/T_∞. In the near-continuum regime at $\delta \sim 10$, the effect of T_w becomes relatively strong at small $Ma = 0.1$ and 0.2.

Thus, the variation of both ζ and $St \cdot Ma$ is dominated only by δ. This fact simplifies the development of the fitting equations for prediction of the average energy transfer coefficient of a sphere under a broad range of conditions. It was already used in the development of the semi-empirical equation for the Nusselt number Nu by Kavanau (1955). This equation was proposed in the form

$$Nu = \frac{Nu_c}{1 + 3.42 \dfrac{Ma}{Pr\, Re} Nu_c}, \tag{5.8}$$

where $Nu_c = Nu_c(Re, Pr)$ is the value of the sphere Nusselt number in the continuum flow regime, Pr is the Prandtl number, which is nearly constant for monatomic gases,

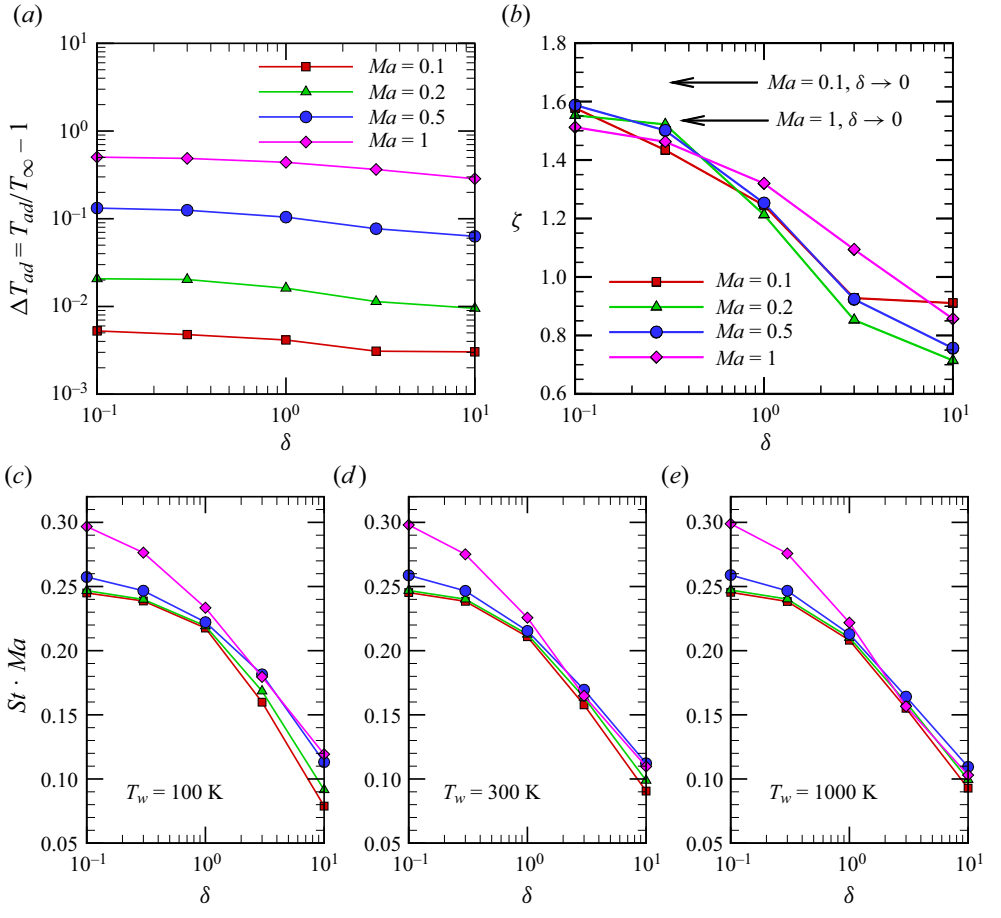

Figure 11. Values of $\Delta T_{ad} = T_{ad}/T_\infty - 1$ (*a*), recovery factor ζ (*b*) and $St \cdot Ma$ (*c–e*) versus density parameter δ at various Ma and T_w obtained for helium with diffuse scattering. In (*b*), horizontal arrows mark the values of ζ in the free-molecular regime at $Ma = 0.1$ and $Ma = 1$.

$Pr \approx 0.67$, and the effects of rarefaction are determined by the parameter $PrRe/Ma \sim Pr\delta$. Equation (5.8) is designed to fit the experimental data for the sphere Nusselt number at $0.1 \leq Ma \leq 0.69$ and $1.75 \leq Re \leq 124$. In this equation, Nu_c can be calculated, for example, with the equation (Eckert & Drake 1959)

$$Nu_c = 2 + 0.459 Pr^{0.33} Re^{0.55}, \tag{5.9}$$

as suggested by Nelson & Fields (1996).

The numerical values of St calculated for $T_w = T_\infty$ are compared with $St = Nu/(PrRe)$ defined by (5.8) in figure 12. The semi-empirical equation by Kavanau (1955) agrees well with the DSMC data points at $Re \geq 1$ in the whole range of the Mach number considered here. At smaller Re, this equation overestimates the Stanton number at $Ma = 0.1$, 0.2 and 0.5, while it somewhat underestimates St at $Ma = 1$ since this equation cannot predict the correct asymptotic behaviour of St in the free-molecular flow regime when $Re \to 0$ at $Ma = const$. Good agreement between the DSMC data points and semi-empirical equation at $Ma = 1$ suggests that the Kavanau (1955) equation can be used to predict the value of St up to $Ma = 1$ in the transitional and continuum regimes at $Re \geq 1$. At relatively

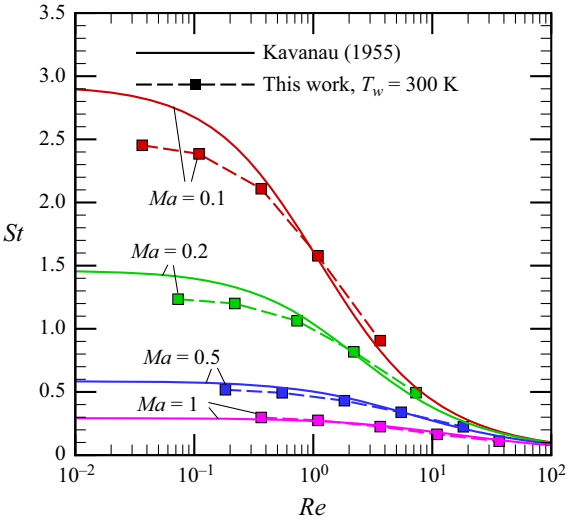

Figure 12. Stanton number St versus Reynolds number Re based on the Kavanau equation (5.8) (solid curves) and obtained with the DSMC method (symbols with dashed curves) at various Ma and $T_w = 300$ K for helium with diffuse scattering.

large subsonic Ma, however, the deviations of T_{ad}/T_∞ from 1 become substantial (see figure 11*a*) so that the calculations of the total energy flux Q require accurate equations for both St and T_{ad}/T_∞.

6. Conclusions

The aerothermodynamic characteristics of a sphere in subsonic flows were calculated by the DSMC method employing *ab initio* potentials for interatomic collisions and the HS molecular model. The calculations were performed for the noble gases helium, neon and krypton over a wide range of gas rarefaction spanning the free-molecular, transitional and continuum regimes for Mach number equal to 0.1, 0.2, 0.5 and 1. The Cercignani–Lampis kernel for gas–surface interaction was used to describe non-diffuse scattering. The parameters of the numerical scheme were chosen to provide numerical errors in the drag coefficient less than 0.5 % at $Ma \geq 0.1$ and in the average energy transfer coefficient less than 1 % at $Ma \geq 0.2$. The effects of several factors, such as gas species, sphere surface temperature and accommodation coefficients, on the flow fields as well as sphere drag and average energy transfer coefficients were studied. The calculated values of the average energy transfer coefficient were used to find the Stanton number and adiabatic temperature of the sphere. The analysis of the numerical results leads to the following conclusions:

(i) In subsonic flows, the aerothermodynamic characteristics of the sphere based on the *ab initio* potentials are close to those based on the HS model if the same parameters of the gas–surface interaction model are used. Thus, the sphere drag and heat transfer in subsonic flows are nearly independent of the gas species but dominated by the parameters of gas scattering at the body surface.

(ii) In the transitional and free-molecular regimes ($\delta \leq 1$), the drag coefficient at $Ma = 0.1$ is close to that obtained from the linearized kinetic equation. In the

near-continuum regime ($\delta = 10$), the difference between the DSMC solutions and linear theory is significant at all values of *Ma* considered.

(iii) The values of the drag and average heat transfer coefficients are strongly sensitive to the accommodation coefficients in the Cercignani–Lampis scattering kernel. The diffuse gas–surface interaction always leads to the largest value of the energy transfer coefficient in comparison with non-diffuse interaction. The drag coefficient exhibits a complex behaviour as a function of the accommodation coefficients. It can be either larger or smaller than the drag coefficient in the case of diffuse scattering. Such a behaviour is predicted by both the DSMC method in the transitional regime and theoretical equations obtained for free-molecular flows.

(iv) Both the DSMC method and theoretical solution for the free-molecular regime show that the drag coefficient increases with increasing sphere surface temperature when the free-stream temperature is constant. The average heat transfer coefficient decreases almost linearly with increasing temperature of the sphere.

(v) The Stanton number and adiabatic sphere temperature, which determine the average energy transfer coefficient of the sphere, after appropriate scaling, exhibit weak dependence on the Mach number and relative sphere temperature. Thus, they demonstrate universal scaling behaviours as functions of the density parameter. This finding may result in the development of a relatively simple fitting equation for the average heat transfer coefficient as a function of all flow parameters.

(vi) In the case of diffuse scattering, the values of the drag coefficient found by the DSMC method when the sphere temperature is equal to the free-stream temperate are in good quantitative agreement with the fitting equation proposed by Loth *et al.* (2021). The fitting equation developed by Henderson (1976) overestimates the drag coefficient in the transitional and near-free-molecular regimes, and the degree of overestimation increases with increasing surface temperature. The fitting equation proposed by Kavanau (1955) for the sphere Nusselt number agrees with the results of the DSMC method when the Reynolds number is greater than 1. At smaller Reynolds numbers, this equation substantially overestimates the DSMC results.

Supplementary material. Supplementary material is available at https://doi.org/10.1017/jfm.2024.1036.

Acknowledgements. F.S. thanks CNPq, Brazil for the support of his research (grant no. 303429/2022-4). A.N.V. acknowledges the support of the present work by the National Science Foundation (USA) through RII-Track-1 Future Technologies and Enabling Plasma Processes project (award OIA-2148653). Computational support is provided by the Alabama Supercomputer Center and Laboratório Central de Processamento de Alto Desempenho of UFPR.

Declaration of interests. The authors report no conflict of interest.

Author ORCIDs.
Felix Sharipov https://orcid.org/0000-0001-9372-2915.

References

Aleksandrov, V.Y. & Fridlender, O.G. 2008 Slow gas motions and the negative drag of a strongly heated spherical particle. *Fluid Dyn.* **43** (3), 485–492.

Aoki, K. & Sone, Y. 1987 Temperature field induced around a sphere in a uniform flow of a rarefied gas. *Phys. Fluids* **30** (7), 2286–2288.

Aziz, R.A., Janzen, A.R. & Moldover, M.R. 1995 *Ab-initio* calculations for helium: a standard for transport property measurements. *Phys. Rev. Lett.* **74** (9), 1586–1589.

Bailey, A.B. 1974 Sphere drag coefficient for subsonic speeds in continuum and free-molecule. *J. Fluid Mech.* **65**, 401–410.

BAILEY, A.B. & HIATT, J. 1971 Free-flight measurements of sphere drag at subsonic, transonic, supersonic, and hypersonic speeds for continuum, transition, and near-free-molecular flow conditions. *Tech. Rep.* AEDC-TR-70-291. Arnold Engineering Development Center Report.

BERESNEV, S.A., CHERNYAK, V.G. & FOMYAGIN, G.A. 1990 Motion of a spherical-particle in a rarefied-gas. Part 2. Drag and thermal polarization. *J. Fluid Mech.* **219**, 405–421.

BIRD, G.A. 1994 *Molecular Gas Dynamics and the Direct Simulation of Gas Flows*. Oxford University Press.

CARLSON, D.J. & HOGLUND, R.F. 1964 Particle drag and heat transfer in rocket nozzles. *AIAA J.* **2**, 1980–1984.

CENCEK, W., PRZYBYTEK, M., KOMASA, J., MEHL, J.B., JEZIORSKI, B. & SZALEWICZ, K. 2012 Effects of adiabatic, relativistic, and quantum electrodynamics interactions on the pair potencial and thermophysical properties of helium. *J. Chem. Phys.* **136** (22), 224303.

CERCIGNANI, C. & LAMPIS, M. 1971 Kinetic model for gas-surface interaction. *Transp. Theory Stat. Phys.* **1**, 101–114.

CERCIGNANI, C. & LAMPIS, M. 1972 Free molecular flow past a flat plate in the presence of a nontrivial gas-surface interaction. *Z. Angew. Math. Phys.* **23**, 713–728.

CERCIGNANI, C., PAGANI, C.D. & BASSANINI, P. 1968 Flow of a rarefied gas past an axisymmetrical body. II. Case of a sphere. *Phys. Fluids* **11** (7), 1399–1403.

CHEN, B., WANG, B., MAO, F., KE, B., WEN, J., TIAN, R. & LU, C. 2020 Review on separation mechanism of corrugated plate separator. *Ann. Nucl. Energy* **144**, 107548.

DAVIS, E.J. 1997 A history of single aerosol particle levitation. *Aerosol Sci. Technol.* **26**, 212–254.

ECKERT, E.R.T. & DRAKE, R.W. 1959 *Heat and Mass Transfer*, 2nd edn. McGraw-Hill.

FILIPPOV, A.V. & ROSNER, D.E. 2000 Energy transfer between an aerosol particle and gas at high temperature ratios in the Knudesn transition regime. *Intl J. Heat Mass Transfer* **43**, 127–138.

GALKIN, V.S., KOGAN, M.N. & FRIDLENDER, O.G. 1972 Flow past a strongly heated sphere by a gas with low Reynolds numbers. *Z. Angew. Math. Mech.* **36** (5), 829–833.

HELLMANN, R., BICH, E. & VOGEL, E. 2008 *Ab initio* potential energy curve for the neon atom pair and thermophysical properties of the dilute neon gas. I. Neon-neon interatomic potential and rovibrational spectra. *Mol. Phys.* **106** (1), 133–140.

HENDERSON, C.B. 1976 Drag coefficients of spheres in continuum and rarefied flows. *AIAA J.* **14** (6), 707–708.

JÄGER, B., HELLMANN, R., BICH, E. & VOGEL, E. 2016 State-of-the-art *ab initio* potential energy curve for the krypton atom pair and thermophysical properties of dilute krypton gas. *J. Chem. Phys.* **144**, 114304.

JOACHAIN, J. 1975 *Quantum Collision Theory*. North-Holland.

KALEMPA, D. & SHARIPOV, F. 2020 Drag and thermophoresis on a sphere in a rarefied gas based on the Cercignani-Lampis scattering model of gas-surface interaction. *J. Fluid Mech.* **900**, A37.

KALEMPA, D. & SHARIPOV, F. 2022 Thermophoretic force on a sphere of arbitrary thermal conductivity in a rarefied gas. *Vacuum* **201**, 111062.

KAVANAU, L.L. 1955 Heat transfer from spheres to a rarefied gas in subsonic flow. *Trans. ASME* **77**, 617–623.

KAYANG, K.W., VOLKOV, A.N., ZHILYAEV, P.A. & SHARIPOV, F. 2023 The *ab initio* potential energy curves of atom pairs and transport properties of high-temperature vapors of Cu and Si and their mixtures with He, Ar, and Xe gases. *Phys. Chem. Chem. Phys.* **25**, 4872–4898.

KIM, Y.W. & YOO, J.Y. 2012 Transport of solid particles in microfluidic channels. *Opt. Lasers Engng* **50** (1, SI), 87–98.

KOSHMAROV, Y.A. & SVIRSHEVSKII, S.B. 1993 *Aero- and Hydromechanics*. Mashinostroenie.

LIMA BERNARDO, B.L., MORAES, F. & ROSAS, A. 2013 Drag force experienced by a body moving through a rarefied gas. *Chinese J. Phys.* **51**, 189–199.

LIU, F., DAUN, K.J., SNELLING, D.R. & SMALLWOOD, G.J. 2006 Heat conduction from a spherical nano-particle: status of modeling heat conduction in laser-induced incandescence. *Appl. Phys.* B **88**, 355–382.

LOTH, E., TYLER DASPIT, J., JEONG, M., NAGATA, T. & NONOMURA, T. 2021 Supersonic and hypersonic drag coefficients for a sphere. *AIAA J.* **59** (8), 3261–3274.

LOYALKA, S.K. 1992 Motion of a sphere in a gas: numerical solution of the linearized Boltzmann equation. *Phys. Fluids* **4** (5), 1049–1056.

MILLIKAN, R.A. 1910 The isolation of an ion, a precision measurement of its charge, and the correction of stokes's law. *Science* **32**, 436–448.

NELSON, H.F. & FIELDS, J.C. 1996 Heat transfer in two-phase solid-rocket plumes. *J. Spacecr. Rockets* **33**, 494–500.

OSEEN, C.W. 1910 Ueber die Stokessche Formel und die verwandte Aufgabe in der Hydrodynamik. *Ark. Mat. Astron. Fys.* **6** (29), 1–20.

OSEEN, C.W. 1913 Uber den Giiltigkeitsbereich der Stokesschen Widerstandsformel. *Ark. Mat., Astron. Fys.* **9** (16), 1–15.

ROOS, F.W. & WILLMARTH, W.W. 1971 Some experimental results on sphere and disk drag. *AIAA J.* **9**, 285–291.

SHAKHOV, E.M. 1968 Generalization of the Krook kinetic relaxation equation. *Fluid Dyn.* **3** (5), 95–96.

SHARIPOV, F. 2012*a* Benchmark problems in rarefied gas dynamics. *Vacuum* **86, SI** (11), 1697–1700.

SHARIPOV, F. 2012*b* Power series expansion of the Boltzmann equation and reciprocal relations for non-linear irreversible phenomena. *Phys. Rev.* E **84** (6), 061137.

SHARIPOV, F. 2016 *Rarefied Gas Dynamics. Fundamentals for Research and Practice*. Wiley-VCH.

SHARIPOV, F. 2022 Direct simulation Monte Carlo method based on *ab initio* potential: recovery of transport coefficients of multi-component mixtures of noble gases. *Phys. Fluids* **34**, 097114.

SHARIPOV, F. & BERTOLDO, G. 2006 Heat transfer through a rarefied gas confined between two coaxial cylinders with high radius ratio. *J. Vac. Sci. Technol.* A **24** (6), 2087–2093.

SHARIPOV, F. & MOLDOVER, M. 2016 Energy accommodation coefficient extracted from acoustic resonator experiments. *J. Vac. Sci. Technol.* A **34** (6), 061604.

SHARIPOV, F. & STRAPASSON, J.L. 2012 *Ab initio* simulation of transport phenomena in rarefied gases. *Phys. Rev.* E **86** (3), 031130.

SHARIPOV, F. & VOLKOV, A.N. 2022 Aerothermodynamics of a sphere in a monatomic gas based on ab initio interatomic potentials over a wide range of gas rarefaction: transonic, supersonic and hypersonic flows. *J. Fluid Mech.* **942**, A17.

STOKES, G.G. 1845 On the theories of the internal friction of fluids in motion and of the equilibrium and motion of elastic solids. *Trans. Camb. Phil. Soc.* **8**, 287–319.

STOKES, G.G. 1851 On the effect of internal friction of fluids on the motion of pedulums. *Trans. Camb. Phil. Soc.* **9**, 8–106.

STOKES, M.A., KHAIRALLAH, S.A., VOLKOV, A.N. & RUBENCHIK, A.M. 2022 Fundamental physics effects of background gas species and pressure on vapor plume structure and spatter entrainment in laser melting. *Additive Manuf.* **55**, 102819.

TAGUCHI, S. & TSUJI, T. 2022 Inversion of the transverse force on a spinning sphere moving in a rarefied gas. *J. Fluid Mech.* **933**, A37.

TAKATA, S., SONE, Y. & AOKI, K. 1993 Numerical analysis of a uniform flow of a rarefied gas past a sphere on the basis of the Boltzmann equation for hard-sphere molecules. *Phys. Fluids* A **5** (3), 716–737.

TROTT, W.M., CASTANEDA, J.N., TORCZYNSKI, J.R., GALLIS, M.A. & RADER, D.J. 2011 An experimental assembly for precise measurement of thermal accommodation coefficients. *Rev. Sci. Instrum.* **82** (3), 035120.

VOLKOV, A.N. 2009 Aerodynamic coefficients of a spinning sphere in rarefied-gas flow. *Fluid Dyn.* **44**, 141–157.

VOLKOV, A.N. 2011 Transitional flow of a rarefied gas over a spinning sphere. *J. Fluid Mech.* **683**, 320–345.

VOLKOV, A.N. & O'CONNER, G.M. 2011 Parallel direct simulation Monte Carlo of two-phase gas-droplet laser plume expansion from the bottom of a cylindrical cavity into an ambient gas. In *Computational Fluid Dynamics 2010* (ed. A. Kuzmin), pp. 105–112. Springer.

VOLKOV, A.N. & SHARIPOV, F. 2017 Flow of a monatomic rarefied gas over a circular cylinder: calculations based on the *ab initio* potential method. *Intl J. Heat Mass Transfer* **114**, 47–61.

VOLKOV, A.N. & STOKES, M.A. 2024 Effects of nanoparticles on plasma shielding at pulsed laser ablation of metal targets. In *Proc. of SPIE, Vol. 12939* (ed. C.R. Phipps & V.E. Gruzdev), p. 1293904. Society of Photo-Optical Instrumentation Engineers.

VOLKOV, A.N., TSIRKUNOV, Y.M. & OESTERLÉ, B. 2005 Numerical simulation of a supersonic gas-solid flow over a blunt body: the role of inter-particle collisions and two-way coupling effects. *Intl J. Multiphase Flow* **31**, 1244–1275.